Using Land Long-Term Data Records to Map Land Cover Changes in China Over 1981–2010

Haixing Li, Pengfeng Xiao, *Member, IEEE*, Xuezhi Feng, Yongke Yang, Lingxiao Wang, Wenbo Zhang, Xiaohui Wang, Weiding Feng, and Xiao Chang

***Abstract*—China has undergone significant land cover changes since the 1980s. However, there are limited consistent and continuous dataset of national scale. Using advanced very high resolution radiometer and moderate resolution imaging spectrometer data from the land long-term data record, we developed a large-scale classification approach to produce a decadal 5-km resolution land cover dataset for China (ChinaLC) from 1981 to 2010. A total of 19 classes of training and validation samples were obtained from visual interpretation of high-resolution Google Earth images and historical vegetation maps. Combined efforts of standard criteria, rigid check, and detailed recording were conducted to strengthen the robustness of the multitemporal samples. The different compositions of metrics and parameters were tested to obtain the optimal support vector machine (SVM) classification results. The ChinaLC dataset has an average overall accuracy of approximately 75%, which is much higher compared with other large-scale land cover datasets. Furthermore, a high consistency was found between the land cover changes of ChinaLC and other studies using higher spatial resolution data. The decadal spatial–temporal transition patterns were analyzed and the important reasons for accelerated landscape changes were also explained over the 30 years.**

***Index Terms*—China, land cover change, land cover classification, land long-term data record (LTDR), support vector machine (SVM).**

I. Introduction

LAND cover is defined as the observed physical cover on the Earth's surface, which includes natural and planted vegetation, forest, human construction, water bodies, barren land or sand surfaces, and snow cover or ice caps [1]. This nonstatic and dynamic variations, resulted from human activity and natural processes, is a crucial variable for studies including climate, conservation biology, soil erosion, hydrology, atmospheric quality, and food security [2].

China has experienced rapid land cover changes from the effect of continued and intense economic globalization together with the "Reform and Opening up" policy from 1978. The phenomenon of urban expansion, extensive land cover transformation, and serious land deterioration [3], [4] made the subsequent decades an important period worthy of detailed investigation. In view of the impacts of global environmental change, only with accurate land cover data will it be possible to improve the performance of ecosystem, hydrological, and climate models at national scale [5].

Remote sensing has been widely recognized as the most economic and feasible approach to derive land cover information over large areas [6]. To date, many global land cover datasets have emerged from different initiatives using satellite data. The main freely available datasets are shown in Table I. Extensive studies focused on land cover mapping include the updated production of land cover datasets [25]–[27], the comparison of classification methods and accuracy assessment [28]–[31], as well as the challenges and efforts [32]–[35].

Comparative analyses of these global land cover datasets have revealed considerable disagreements and uncertainties [36], [37]. One of the major drawbacks of the datasets is the lack of interoperability among them. Since their development has been driven by different national or international initiatives, they have been developed for different purposes and hold diverse technical characteristics. Many of these classifications, however, were aimed at a particular project and are often not comparable with each other. Each was produced using different data inputs and algorithms; therefore, they were not designed to be comparable and exist as independent datasets with low overall consistency. Agreement on the global distribution of individual land cover classes is limited, although in many cases, a reasonable agreement exists at a global level in terms of the total area and general spatial patterns [38].

In our previous study, GLC2000, IGBP-DISCover, MCD12Q1 2001, UMD, and GlobCover 2005 were evaluated over China [39]. The results indicated that disagreement existed among the datasets over large areas. There are several possible reasons for the low consistency of the datasets:

1) a limited number of valid samples in China is the main reason for low accuracy and consistency;

Manuscript received May 25, 2016; revised September 8, 2016 and November 12, 2016; accepted December 12, 2016. Date of publication January 9, 2017; date of current version March 22, 2017. This work was supported in part by the National Natural Science Foundation of China under Grant 41671344, in part by the National Key Basic Research Program on Global Change under Grant 2011CB952001, and in part by the Qinglan Project of Jiangsu Province under Grant 201423. *(Corresponding author: Pengfeng Xiao.)*

The authors are with the Department of Geographic Information Science, Nanjing University, Nanjing 210023, China, with the Collaborative Innovation Center of South China Sea Studies, Nanjing 210023, China, and also with the Jiangsu Center for Collaborative Innovation in Geographical Information Resource Development and Application, Nanjing 210023, China (e-mail: leehaixing@126.com; xiaopf@nju.edu.cn; xzf@nju.edu.cn; yangyk198734@126.com; rebecxiao@gmail.com; wenbo19870515@163.com; xiaohuiwang1989@163.com; njdxfwd@126.com; ziyuanhuayu@gmail.com).

Color versions of one or more of the figures in this paper are available online at http://ieeexplore.ieee.org.

Digital Object Identifier 10.1109/JSTARS.2016.2645203

TABLE I
MAIN FREELY AVAILABLE GLOBAL LAND COVER DATASETS

Name	Data source	Spatial resolution	Year	Classification method	Classification scheme	Validation data	Overall accuracy
IGBP-DISCover	AVHRR [7]	1 km	Apr. 1992–Mar. 1993	Unsupervised clustering with postclassification refinement	IGBP 17 classes	Landsat TM and SPOT images	66.9% [16]
UMD	AVHRR [4]	1 km	Apr. 1992–Mar. 1993	Supervised decision tree	IGBP 14 classes	Other digital datasets	69% [17]
GLC2000	SPOT-4 VEGETATION [8], [9]	1 km	Nov. 1999–Dec. 2000	Unsupervised classification	LCCS 22 classes	High resolution satellite data and ancillary information	$68.5 \pm 5\%$ [18]
MCD12Q1	MODIS [9], [10]	1 km	2001, 2010	Supervised classification and single class extraction	IGBP 17 classes	High-resolution land cover information	75% [19]
GLCNMO	MODIS [11]	500 m	2003, 2008	Supervised classification and single class extraction	LCCS 20 classes	Landsat, MODIS NDVI, Google Earth	76.5% [20]
GlobCover	MERIS [12]	300 m	2005, 2009	Unsupervised classification	LCCS 22 classes	SPOT-VEGETATION NDVI, Virtual Earth/Google Earth	67.1% [21]
CCI-LC	MERIS, SPOT, MODIS, ASAR	300 m	2000 (1998–2002), 2005 (2003–2007), 2010 (2008–2012)	Supervised and unsupervised classification	LCCS 22 classes	Systematic sampling of the TREES dataset by external parties	70.8% [22]
FROM-GLC	Landsat TM /ETM+ [14]	30 m	$\sim 2000, \sim 2010$	Supervised classification	11 classes	Landsat TM/ETM+	69.50% [23]
GlobeLand30	Landsat TM/ETM+, HJ-1	30 m	2000, 2010	Pixel- and object-based classification	10 classes	Google Earth, Landsat TM/ETM+, Degree Confluence Project	83.51% [24]

2) a greater landscape heterogeneity can significantly complicate the spectral characteristics of the Earth's surface, rendering land cover mapping less accurate;
3) the disparities in data source, classification method, and classification scheme result in low consistency among different datasets [40]; and
4) the different years of the land cover datasets may also result in disagreement within these datasets.

The existence of these discrepancies hinders the development of a reliable land cover dataset over China for accurate climate change and other environmental studies, indicating the need for improved national land cover data [7]. As a result, we produced a decadal 5-km resolution land cover dataset for China (ChinaLC) with a time span of 30 years: from 1981 to 2010. Our aims included:

1) finding a suitable data source documenting the 30 years of national land cover changes;
2) using a strategy to compensate for a lack of references;
3) producing a dataset with a consistent spatial resolution, taking into account the deviation of results from different sensors;
4) ensuring consistency in the classification results; and
5) overcoming issues relating to the accuracy and accessibility of recent national-scale samples.

II. STUDY AREA AND DATA

A. Study Area

The study area spans $\sim 8670\,\mathrm{km}^2$ across East Asia, including the entire territory of China and parts of Russia, Central Asia, and Southeast Asia. In order to produce input parameters for climate models, we included a rectangular area that extended from 48°24′8″N to 0°53′17″S and from 38°29′20″E to 178°28′48″E. However, we focused only on China for the analyses of classification results. Generally, this area experiences a temperate climate with cold winters and warm summers. Specifically, the Eastern China, located in eastern Asia and facing the Pacific Ocean, displays strong seasonal monsoons and significant variations in temperature. Plenty of rainfall enable intensive agriculture cycles and diversified vegetation classes. The western China, located in center of the largest continent, has an arid continental climate. The rugged topography of the Tibetan Plateau also results in a complex land cover types over there.

B. Data for Classification

The National Aeronautics and Space Administration land long-term data record (LTDR) project reprocesses the global area coverage (GAC) dataset from 1981 to the present for the whole globe. Specifically, it creates daily surface reflectance product as a fundamental climate data record, and derives daily normalized difference vegetation index (NDVI) and leaf area index/fraction of absorbed photosynthetically active radiation as two thematic climate data records.

As shown in Table II, the LTDR archive (ID 1–4) was selected as the main data source for producing the proposed dataset for reasons:

1) the GAC is the only available dataset with dynamic data continuity from 1981 to 2010;
2) the GAC is reprocessed by applying the preprocessing improvements identified in the Pathfinder advanced very

TABLE II
DATA SOURCES USED FOR PRODUCING THE CHINALC DATASET

ID	Data source	Main usage	Year	Resolution/Scale
1	LTDR GAC reflectance data	Reflectance for metric calculation	1981–1999	5 km
2	LTDR MOD09CMG	Reflectance for metric calculation	2000–2010	1 km
3	LTDR NDVI data	Vegetation indexes for metric calculation	1981–1999	5 km
4	LTDR AVH13C1 monthly global vegetation indices	Vegetation indexes for metric calculation	2000–2010	1 km
5	Chinese Vegetation Map	Reference data for vegetation sample selection	1980s	1:4 000 000
6	Chinese Vegetation Map	Reference data for vegetation sample selection	1990s	1:1 000 000
7	ASTER GDEM	Elevation, aspect, and slope for metric calculation	2009	1 km
8	DMSP-OLS nighttime data	Urban and built-up area extraction	1981–2010	500 m
9	Google Earth images	High resolution images for sample selection	2000–2010	<10 m
10	Google Earth images	Landsat images for sample selection	1981–2010	<10 m
11	Panorama photos and historical documents	Auxiliary data for visual interpretation of samples	1981–2010	–

high resolution radiometer (AVHRR) Land II project and the atmospheric corrections used in the moderate resolution imaging spectrometer (MODIS) preprocessing [41]; and

3) repeated quality assurances have been implemented such as radiometric in-flight vicarious calibration, inverse navigation, and atmospheric corrections [42].

Generally, the GAC represents a credible and high-quality data source that is suitable for studying the 30-year dynamics of land use trends. The version 3 of LTDR dataset (http://ltdr.nascom.nasa.gov) was used in the study, including the daily reflectance and NDVI data from June 1981 to December 2010.

Furthermore, studies have indicated that using spectral images alone is insufficient for accurate land-cover classification. Adding the topographic data as alternative metrics has been shown to effectively improve the accuracy [43]. Thus, the version 1 of advanced spaceborne thermal emission and reflection radiometer (ASTER) global digital elevation model (GDEM) dataset [44] (https://wist.echo.nasa.gov) was used in the study and derived into 5-km elevation and aspect data in order to match the LTDR dataset.

Finally, because of the small sizes of urban areas relative to the total land area, they are difficult to detect at the national scale using coarse-resolution optical remote sensing. Fortunately, the defense meteorological satellite program operational linescan system (DMSP-OLS) nighttime light data are capable of effectively mapping urban areas at regional or global scales [45]. Thus, the annual average nighttime light dataset (http://www.ngdc.noaa.gov/eog/dmsp.html) was used to depict urban and built-up areas.

C. Auxiliary Data for Generating Samples

Multisource auxiliary data including historical vegetation maps, high or medium resolution images, panorama photos, and documents were used to depict training and validation samples at different phases.

The 1:4 000 000 vegetation map of China was used as reference for the 1980s, which realistically depicts the national geographical distribution of natural and agricultural vegetation. It was digitized from the vegetation data collected from 1972 to 1976 [46]. Likewise, the 1:1 000 000 vegetation map of China

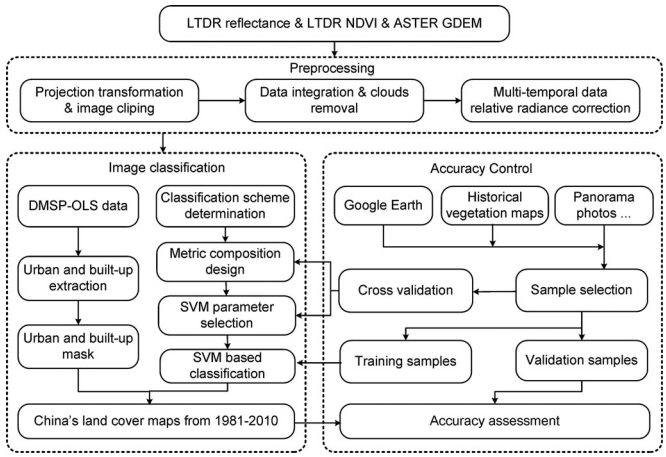

Fig. 1. Flowchart of the production of the ChinaLC dataset.

was used as the reference historical data for the 1990s [47]. It was digitized from the Chinese vegetation map of 2001. These two maps were provided by the Environmental and Ecological Science Data Center for West China.

Meanwhile, we used Google Earth (GE) as the main data source for the selection of training and validation samples from 2000 to 2010. Based on the availability, quality, and date of procurement, GE superimposes widely distributed high-resolution images over coarser images which are easy to navigate and free to access. These images cover more than 20% of the Earth's land surface and more than a third of the human population [48]. Another advantage of GE over other map services accessed within webpages (e.g., Google Maps, Microsoft Bing) is that historical high-resolution images before 2000 are available, allowing temporal sampling that can span ten or more years. Besides, the panorama photos and historical documents were also helpful for better identification of samples.

III. METHODOLOGY

In order to produce a decadal land cover dataset for China from 1981 to 2010, we developed a new large-scale land cover classification approach based on the LTDR dataset. A suitable classification scheme was determined to adapt to China's land cover classes and to be compatible with other datasets.

TABLE III
CLASSIFICATION SCHEME OF THE CHINALC DATASET, ADAPTED FROM 17-CLASS IGBP SCHEME [7], [10], [11]

ID	Class	Description
1	Evergreen Needleleaf Forest	Lands dominated by trees with a percent canopy over 60% and height exceeding 2 m. Almost all trees remain green all year. Canopy is never without green foliage.
2	Evergreen Broadleaf Forest	Lands dominated by trees with a percent canopy cover $>60\%$ and height exceeding 2 m. Almost all trees remain green all year. Canopy is never without green foliage.
3	Deciduous Needleleaf Forest	Lands dominated by trees with a percent canopy cover $>60\%$ and height exceeding 2 m. Consist of seasonal needle-leaf tree communities with an annual cycle of leaf-on and leaf-off periods.
4	Deciduous Broadleaf Forest	Lands dominated by trees with a percent canopy cover $>60\%$ and height exceeding 2 m. Consist of seasonal broad-leaf tree communities with an annual cycle of leaf-on and leaf-off periods.
5	Mixed Forest	Lands dominated by trees with a percent canopy cover $>60\%$ and height exceeding 2 m. Consist of tree communities with interspersed mixtures or mosaic of the other four forest cover classes. None of the forest classes exceed 60% of the landscape.
6	Closed Shrubland	Lands dominated by bushes or shrubs. Bush and shrub percent canopy cover is $>40\%$. Bushes do not exceed 5 m in height. Shrubs or bushes can be either evergreen or deciduous. Tree canopy cover is $<10\%$. The remaining cover is either barren or herbaceous.
7	Open Shrubland	Lands dominated by shrubs. Shrub canopy cover is $>10\%$ and $<40\%$. Shrubs do not exceed 2 m in height and can be either evergreen or deciduous. The remaining cover is either barren or of annual herbaceous class.
8	Woody Savannas	Lands with herbaceous and other understorey systems, and with forest canopy between 30% and 60%. The forest cover height exceeds 2 m.
9	Savannas	Lands with herbaceous and other understorey systems, and with forest canopy between 10% and 30%. The forest cover height exceeds 2 m.
10	Grassland	Lands with continuous herbaceous cover and $<10\%$ tree or shrub canopy cover.
11	Permanent Wetlands	Lands with a permanent mixture of water and herbaceous or woody vegetation that covers extensive areas. The vegetation can be present in either salt, brackish, or fresh water.
12	Tundra	Lands where the subsoil is permafrost, or permanently frozen soil, or refers to the treeless plain in general.
13	Urban and Built-up	Land covered by buildings and other man-made structures. Note that this class will not be mapped from the LTDR imagery but will be developed from the DMSP-OLS nighttime light data.
14	Cropland/Natural Vegetation Mosaic	Lands with a mosaic of cropland, forest, shrub lands, and grassland in which no one component comprises more than 60% of the landscape.
15	Snow and Ice	Lands under snow and/or ice cover throughout the year.
16	Barren	Lands of exposed soil, sand, rocks, or snow that never have more than 10% vegetated cover during any time of the year.
17	Water Bodies	Oceans, seas, lakes, reservoirs, and rivers. Can be either fresh or salt water.
18	Irrigated Cropland	Lands of cropland with ridge and water storage, where aquatic crops such as rice, especially in paddy fields, or others are grown.
19	Rainfed Cropland	Lands of cropland without irrigation equipment, where xeromorphic crops, which basically depend on rain, are grown.

Reflectance and NDVI data were then preprocessed to produce monthly integrated cloud-free images with the Lambert conformal conic projection. The multitemporal relative radiance correction was conducted for consistence. Guiding by criteria, multisource referenced data were uniformly selected for a visual interpretation of the training and validation samples. The best metrics were then determined from different compositions, indicating the best accuracy and efficiency for distinguishing land cover classes. A support vector machine (SVM) based classification method was selected to produce the primary land cover dataset using parameters with the highest cross validation accuracy. Efforts were made to modify the potential omission that existed in the preliminary result from the SVM classification. Finally, the accuracy of the proposed method was assessed by validation samples, also including reference data extracted from higher-resolution data (see Fig. 1).

A. Classification Scheme

The classification scheme (see Table III) was developed based on the 17-class IGBP scheme [7], [10], [11], because it is required by the climate model and widely used by datasets such as IGBP-DISCover, UMD, and MCD12Q1. The commonly used IGBP scheme is exhaustive and exclusive [49], which embraces a canopy component philosophy and climate independence [50]. It has also been modified to be compatible with the present classification schemes for environmental modeling.

We made the following modifications to the IGBP scheme:

1) the cropland category was subdivided into "irrigated cropland" and "rainfed cropland." China's agricultural sector uses unique cultivation methods to transition between irrigated cropland and rainfed cropland, and the differences were found to increase during the study period [51]. Crop productivity and water composition also differ significantly between these two classes of cropland [52]. These differences in ambiguous reflectance features could result in erroneous climate simulations, e.g., incorrect relative contributions of different cropland to evapotranspiration to the atmosphere [53]; and
2) the tundra class was added to the scheme owing to a significant carbon contribution to ecosystems. Tundra areas exist at high altitudes in the north of the study area and methane emissions from tundra areas contribute $\sim 10\%$ to the global atmospheric budget [54].

B. Data Integration and Cloud Removal

To fill the missing data and remove the undesired noise effects after radiometric and geometric corrections, monthly composite images were generated from the component images of 30 consecutive days from 1981 to 2010. As described in our previous work [42], the fact that clouds are generally bright in visible channels and cold in thermal channels is the basic principle of this composition method. The process was conducted by

TABLE IV
ALTERNATIVE METRICS DESIGNED FOR THE PROPOSED LAND COVER CLASSIFICATION, ADAPTED FROM [5]

ID	Metrics description	ID	Metrics description	ID	Metrics description
1	Maximum NDVI value	17	Channel 1 value from month of maximum NDVI	33	Maximum channel 4 value of 8 greenest months
2	Minimum NDVI value of 8 greenest months	18	Mean channel 1 value of 4 warmest months	34	Minimum channel 4 value of 8 greenest months
3	Mean NDVI value of 8 greenest months	19	Channel 1 value of warmest month	35	Mean channel 4 value of 8 greenest months
4	Amplitude of NDVI over 8 greenest months	20	Maximum channel 2 value of 8 greenest months	36	Amplitude of channel 4 over 8 greenest months
5	Mean NDVI value of 4 warmest months	21	Minimum channel 2 value of 8 greenest months	37	Channel 4 value from month of maximum NDVI
6	NDVI value of warmest month	22	Mean channel 2 value of 8 greenest months	38	Mean channel 4 value of 4 warmest months
7	Maximum EVI value	23	Amplitude of channel2 over 8 greenest months	39	Channel 4 value of warmest month
8	Minimum EVI value of 8 greenest months	24	Channel 2 value from month of maximum NDVI	40	Maximum channel 5 value of 8 greenest months
9	Mean EVI value of 8 greenest months	25	Mean channel 2 value of 4 warmest months	41	Minimum channel 5 value of 8 greenest months
10	Amplitude of EVI over 8 greenest months	26	Channel 2 value of warmest month	42	Mean channel 5 value of 8 greenest months
11	Mean EVI value of 4 warmest months	27	Maximum channel 3 value of 8 greenest months	43	Amplitude of channel 5 over 8 greenest months
12	EVI value of warmest month	28	Mean channel 3 value of 8 greenest months	44	Channel 5 value from month of maximum NDVI
13	Maximum channel 1 value of 8 greenest months	29	Amplitude of channel 3 over 8 greenest months	45	Mean channel 5 value of 4 warmest months
14	Minimum channel 1 value of 8 greenest months	30	Channel 3 value from month of maximum NDVI	46	Channel 5 value of warmest month
15	Mean channel 1 value of 8 greenest months	31	Mean channel 3 value of 4 warmest months	47	Elevation value
16	Amplitude of channel over 8 greenest months	32	Channel 3 value of warmest month	48	Aspect value

Note: 1) the 8 greenest months are selected from March to October per year; 2) the 4 warmest months are selected from June to September; 3) the month of maximum NDVI and EVI is August within China; 4) the warmest month is selected as July; and 5) the channel number represents the AVHRR surface reflectance data for channels 1, 2, 3, and the top of atmosphere (TOA) brightness temperature for channels 4, 5 from 1981 to 2000, and the corresponding MODIS surface reflectance data for channels 1, 2, 20, and the TOA brightness temperature for channels 31, 32 from 2001 to 2010.

1) using the maximum bright temperature of the thermal channel to remove the pixels with potential cloud or cloud shadow to composite the reflectance images;
2) replacing the residual cloudy pixels within water areas with the pixels of the maximum visible channel/thermal channel that were not removed in the previous step; and
3) following the same approach, replacing the pixels with the maximum NDVI of 30 consecutive days to composite the NDVI data.

We applied the composition method on the time series consisting of more than 480 reflectance data (four periods of data, $\sim$120 acquisitions per year, one observation every three days) and more than 96 NDVI data (four periods of data, $\sim$24 acquisitions per year, one observation every 15 days) from 1981, 1990, 2000, and 2010. Finally, the integrated and cloud-free reflectance and NDVI data, thus, consisted of 12×4 observations representing the interannual average and variance of land cover changes.

C. Metric Design

A successful detection of land cover requires appropriate classification metrics [5], [55]. First, spectrotemporal statistical metrics are viable means for discriminating land cover classes [56]. Multitemporal spectral data in the same or consecutive years can be considered as statistical metrics, which in turn can function as descriptive variables that improve the separability between land cover classes. Therefore, as shown in Table IV, the metrics of ID 13–46 were calculated or recomposed by reflectance and brightness temperature values in individual bands.

Second, vegetation indexes (VIs) were included. Most phenology studies use VI time series to derive phenological metrics to identify critical measures that match phenological phases of vegetation development [57]. The mean NDVI reflects the basic growth curve of vegetation, and the maximum, minimum, and amplitude of NDVI reflect the class-specific dependence on interannual changes in climatic drivers. Thus, the NDVI, including its mean, maximum, minimum, and amplitude, is indispensable in the effective identification of deciduous and evergreen vegetation [58], [59]. As shown in the metrics of ID 1–6, the annual maximum, minimum, mean, and amplitude of NDVI were calculated or recomposed as alternative metrics. In the metrics of ID 7–9, the maximum, minimum, mean, and amplitude of enhanced vegetation index (EVI) were added as alternative metrics.

Third, the timing and greenness for the start, peak, and end of the growing season helps to represent vegetation interactions with climate-based factors [60]. Researchers have suggested the use of metrics that describe an annual NDVI temporal profile,

TABLE V
TRAINING AND VALIDATION SAMPLES FOR THE PROPOSED LAND COVER CLASSIFICATION

ID	Class	Number of training samples	Pixels of training samples	Average pixels of training samples	Number of validation samples	Pixels of validation samples	Average pixels of validation samples
1	Evergreen Needleleaf Forest	90	492	5.47	24	149	6.20
2	Evergreen Broadleaf Forest	109	592	5.43	28	56	12.00
3	Deciduous Needleleaf Forest	75	402	5.36	19	198	10.42
4	Deciduous Broadleaf Forest	106	571	5.39	27	220	8.16
5	Mixed Forest	88	490	5.57	22	127	5.76
6	Closed Shrubland	81	1535	18.95	20	61	3.05
7	Open Shrubland	105	707	6.74	27	113	4.20
8	Woody Savannas	28	142	5.08	7	35	5.00
9	Savannas	24	122	5.09	5	25	5.00
10	Grassland	139	1174	8.45	35	257	7.36
11	Permanent Wetlands	63	317	5.04	16	85	5.31
12	Tundra	25	128	5.12	4	18	4.50
13	Urban and Built-up	-	-	-	25	65	2.60
14	Cropland/Natural Vegetation Mosaic	123	627	5.10	31	114	3.68
15	Snow and Ice	85	425	5.00	21	105	5.04
16	Barren	123	615	5.00	31	186	6.02
17	Water Bodies	119	595	5.00	30	190	6.34
18	Irrigated Cropland	115	600	5.22	29	155	5.32
19	Rainfed Cropland	119	690	5.80	30	179	5.96

Note: The training sample for the "urban and built-up" is null since this land cover class was thematically extracted.

such as growing season length and the rate of greenup, rather than direct NDVI values and a rule-based approach to determining land cover classes [61]. Therefore, all the NDVI, EVI, and reflectance of channels in the eight greenest months (from March to October) and the four warmest months (from June to September) were selected from the 12-monthly data in order to emphasize the vegetation growing season and highlight the vegetation interactions that influence land cover classes.

Finally, to overcome the insufficiency of spectral data for land cover classification, topographic data were added as alternative metrics. Specifically, we added the elevation and aspect value calculated from ASTER GDEM. This is due to their representation of temperature variables, incident angle, and sunshine duration [62]. These factors influence the vegetation distribution under different topographic conditions.

D. Sampling Data Selection

The land cover samples in 1981 and 1990 were conducted with help from field-investigation vegetation maps collected in the 1980s [43] and 1990s [44]. The distributions of 868 basic vegetation units were recorded in the vegetation maps, including 11 vegetation classes: needleleaf forest, mixed forest, broadlead forest, shrub, desert, steppe, grass-forb community, meadow, swamp, alpine vegetation, and cultural vegetation. This vegetation scheme was reclassified to match the proposed classification scheme. Available Landsat MSS and TM images from 1981 to 1990 were also used as an auxiliary reference to interactively identify land cover class. The land cover samples were annually chosen in stable areas of the image with pure texture or color to avoid areas of potential change and from dormant season (May to August). In these months, the vegetation is supposed to be fully developed and thus representative for the definition of land cover classes. The visual interpretation of land cover samples in 2000 and 2010 was conducted manually from GE. The available images of QuickBird, IKONOS, or WorldView were used as main reference for visual interpretation. Totally, we collected 2047 samples, each class with an average of 110 samples separately (see Table V). The principles for sample collection were as follows (see Fig. 2).

First, the samples were visually extracted only in homogeneous areas of $\sim$100–225 km^2 (4–9 pixels of 5 km resolution). Areas containing mixed land cover classes were avoided as much as possible.

Second, a uniform distribution of samples was attempted concerning the uneven distribution of available GE high-resolution images. A hollow grid network was built and overlaid on the GE. The number of samples of each class in each grid (500 km $\times$ 500 km) was controlled to be averaged. These procedures were conducted for the main classes (e.g., forests and croplands) as far as possible. For other small areal and regional distributed classes, we put effort to sparsely extract the most typical samples.

Third, multisource reference data were integrated to assist sample selection:

1) GE high-resolution images were available for land cover identification and sample extraction in 2000 and 2010;
2) the vegetation maps were overlain as target areas with the Landsat images on GE, which helps to interactively identify land cover class without high-resolution images;
3) panoramic photos and historical documents on the local geography were used to validate samples where land cover classes remained difficult to identify even in the high-resolution images; and
4) if needed, additional Internet-based research was conducted in order to reduce uncertainty.

Finally, along with the interpretation of preliminary samples, we recorded information related to each sample, i.e., land cover

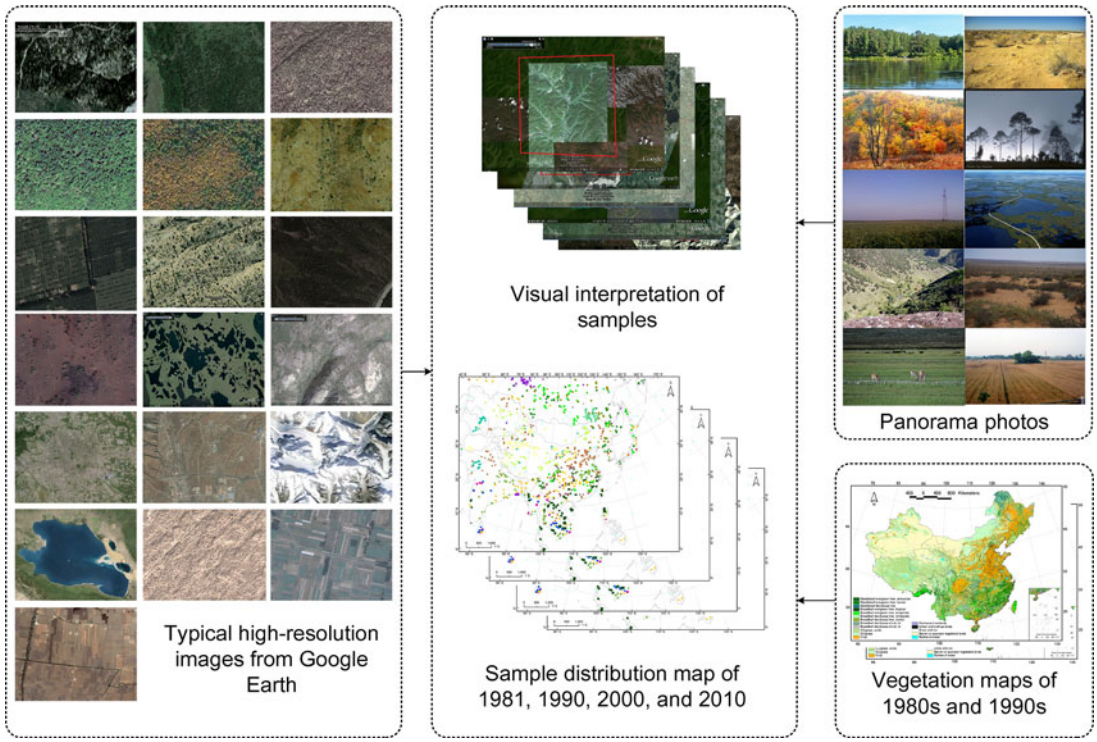

Fig. 2. Proposed sample selection approach for the proposed land cover classification.

class, multiple views of corresponding high-resolution images, panoramic photos, and spatial location. Then, collaborative decisions were made by nine experts participating in the project to verify each preliminary sample according to the sample reports. Only samples on which at least six experts agreed were used for further analysis.

E. Land Cover Classification

We applied an SVM algorithm to conduct land cover classification. The SVM is a supervised machine learning algorithm developed on the basis of statistical learning theory [63]. It is extensively applied for classification and regression with hyper-dimensional space as one of the most stable and efficient classifiers [64], [65].

The quality of the proposed samples is more suitable for the nonparametric classification algorithm, which has no requirement for samples to have Gaussian distribution [66]. Research has indicated that, when compared to conventional nonparametric classification algorithms, SVM generates higher accuracies [67]. Many studies have also validated the suitability of the SVM for images with the similar spatial resolution as our dataset [68], [69].

The procedure of the classification was as follows:

1) the different compositions of the alternative 48 metrics were processed by normalization, and the principal component analysis (PCA) was used to reduce the redundancy of the metrics;
2) the radial basis function kernel was used as it only requires two parameters, i.e., penalty parameter C and kernel width g, and is known to achieve reliable results [70];

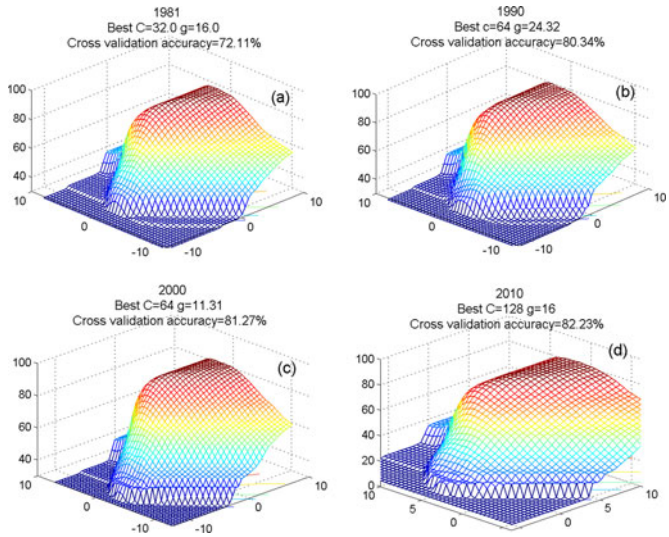

Fig. 3. Proposed parameter selection and cross validation accuracy in 1981 (a), 1990 (b), 2000 (c), and 2010 (d).

3) the grid search approach and cross validation were used together to find the best C and g by specifying the parameter space, the range of C and g, and stopping tolerance; and
4) the "k-fold cross-validation" method was used to divide the samples into ten subsets. The advantage was that it covered every single sample as training and validation sample, and each one of them was validated once. After repeating the cross validation ten times, the average accuracy value was determined.

TABLE VI
PERFORMANCE OF DIFFERENT METRIC COMBINATIONS FOR THE PROPOSED LAND COVER CLASSIFICATION

Year	Metric combination	Best C	Best g	Cross validation accuracy (%)	Running time (h)
1981	NDVIs+EVIs	8	13.68	55.89	3.95
	NDVIs+EVIs (PCA)	16	128	53.76	2.37
	Reflectance+NDVIs+EVIs	32	5.65	68.00	8.51
	Reflectance +NDVIs+EVIs (PCA)	90.51	16	67.21	5.38
	Reflectance+NDVIs+EVIs+DEM	32	16	72.11	11.34
	Reflectance+NDVIs+EVIs+DEM (PCA)	32	8	71.07	5.50
1990	NDVIs+EVIs	16	64	60.23	3.26
	NDVIs+EVIs (PCA)	53.18	128	55.58	2.09
	Reflectance+NDVIs+EVIs	64	73.65	69.65	6.56
	Reflectance +NDVIs+EVIs (PCA)	32	64	69.56	5.79
	Reflectance+NDVIs+EVIs+DEM	64	24.32	80.34	10.78
	Reflectance+NDVIs+EVIs+DEM (PCA)	32	8	79.56	5.68
2000	NDVIs+EVIs	8	128	70.19	3.16
	NDVIs+EVIs (PCA)	128	64	68.40	2.823
	Reflectance+NDVIs+EVIs	90.51	64	78.96	10.38
	Reflectance +NDVIs+EVIs (PCA)	64	15.37	77.54	4.26
	Reflectance+NDVIs+EVIs+DEM	64	11.31	81.27	11.59
	Reflectance+NDVIs+EVIs+DEM (PCA)	22.63	11.31	80.59	6.59
2010	NDVIs+EVIs	16	24.18	71.35	3.75
	NDVIs+EVIs (PCA)	32	64	69.07	2.21
	Reflectance+NDVIs+EVIs	32	14.36	79.61	9.68
	Reflectance +NDVIs+EVIs (PCA)	64	128	76.23	4.67
	Reflectance+NDVIs+EVIs+DEM	128	16	82.23	10.89
	Reflectance+NDVIs+EVIs+DEM (PCA)	64	2.83	81.40	5.67

Parameter optimization was accomplished through a combination of LibSVM, Python SVM, and Gnuplot tools [71]. The best values for the parameters in the four phases are marked in Fig. 3. Each point on the curved surface has a corresponding log2g, log2C, and cross validation accuracy value. Through the grid-search method, the best C and g were found with the highest accuracy. The grid search was repeated to test the performance of different compositions of alternative metrics. The running time, SVM parameters, and cross validation accuracy of these alternative metrics before and after applying the PCA are recorded in Table VI. The metric combination of reflectance, NDVIs, EVIs, and DEM has the highest cross validation accuracy in the four phases.

F. Classification Improvement

Classification results were improved in two ways. First, the relative radiometric correction, with no need for original atmospheric parameters, was used to diminish the exogenous error in different periods. Multitemporal images are not often comparable in terms of radiometric characteristics due to atmospheric scattering and absorption, changes in the atmospheric conditions, variations in solar illumination conditions, and radiometric performance. Therefore, in the case of the multitemporal analysis for change detection, any two datasets must be adjusted to compensate for radiometric divergence [72].

Second, thematic extraction was used on urban and built-up class because of the difficulties in identifying subpixels with urban proportions of less than 75%, which renders it nearly impossible to extract urban samples from optical satellite images at a resolution of 5 km. In this study, urban and built-up class was extracted thematically from the DMSP-OLS nighttime light data. As shown in our previous work [73], nighttime light and NDVI data were subjected to a local SVM-based region-growing method to semi-automatically distinguish urban pixels from the nonurban background in each economic region. The method effectively weakened the blooming effect of the nighttime light data. The thematically extracted urban and built-up results were then resampled to be consistent with the proposed classification results. Then, we applied the mask of urban and built-up on the preliminary SVM-based results.

IV. RESULTS

A. Classification Accuracy Assessment

The proposed approach produced land cover maps of China for 1981, 1990, 2000, and 2010 (see Fig. 4). The classification accuracy was estimated by a confusion matrix. The overall accuracies and Kappa coefficients calculated from 431 validation samples (2388 pixels) for the ChinaLC maps are listed in Table VII.

Given the compatible spatial resolutions and classification schemes, IGBP-DISCover, UMD, GLC2000, MOD12Q1 2000/2010, and GlobCover 2009 were compared with the ChinaLC dataset [74]. Comparisons were made using the same validation samples, as long as their acquisition phases were close to the ChinaLC dataset. The ChinaLC dataset has higher overall accuracy and Kappa coefficient in each period, which validates the effectiveness of the proposed approach.

The spatial consistency comparison was made in the four periods by conducting per-pixel comparisons. The pixels with the same land cover class in different datasets retained their values, whereas pixels with a different land cover class were labeled as a disagreement. The overall agreements were 83.68%

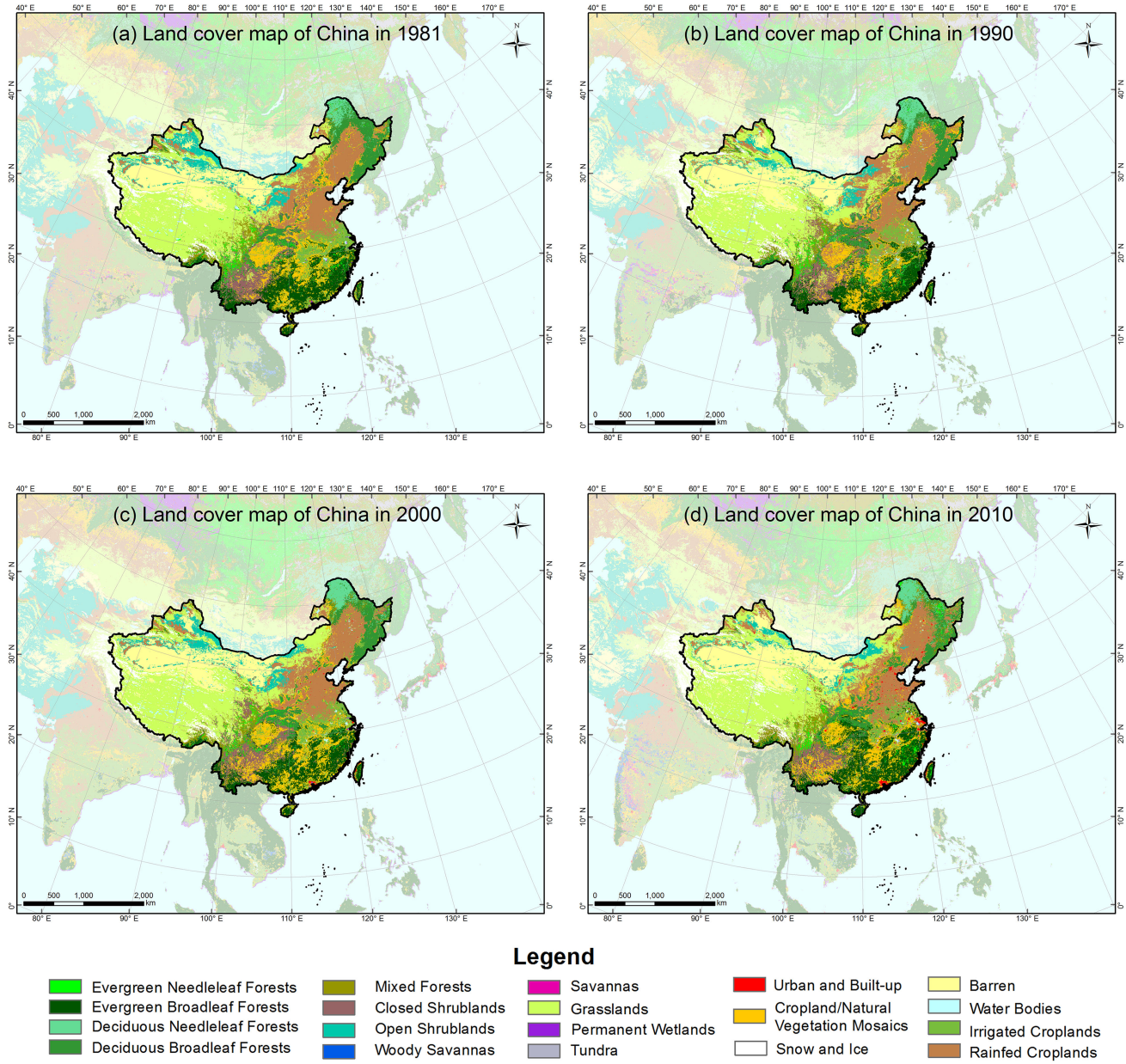

Fig. 4. Land cover maps of China in (a) 1981; (b) 1990; (c) 2000; and (d) 2010.

TABLE VII
OVERALL ACCURACIES AND KAPPA COEFFICIENTS BETWEEN THE CHINALC DATASET AND OTHER LARGE-SCALE LAND COVER DATASETS

Year	Land cover dataset	Overall accuracy (%)	Kappa coefficient
1981	ChinaLC	**71.72**	**0.70**
1990	ChinaLC	**71.94**	**0.70**
1992–1993	IGBP-DISCover	39.80	0.33
1992–1993	UMD	33.00	0.27
2000	ChinaLC	**75.60**	**0.74**
2000	GLC2000	51.70	0.46
2000	MOD12Q1	38.10	0.32
2009	GlobCover	42.40	0.36
2010	MOD12Q1	58.83	0.60
2010	ChinaLC	**78.91**	**0.77**

from 1981 to 1990, 84.07% from 1990 to 2000, and 85.61% from 2000 to 2010. The overall agreement of the four periods was 75.48%.

Of the 182 misclassified samples, most belonged to mixed forest, closed shrubland, savannas, woody savannas, and cropland/natural vegetation mosaic. Producer accuracy was lowest for cropland/natural vegetation mosaic and highest for water bodies. Savannas had the lowest user accuracy while urban and built-up and tundra had the highest. Most misclassified (omitted) samples of cropland/natural vegetation mosaic were transferred to irrigated cropland. The lower accuracy for cropland/natural vegetation mosaic was due to confusion between irrigated cropland, rainfed cropland, and evergreen broadleaf forest, while most misclassified irrigated cropland were confused with

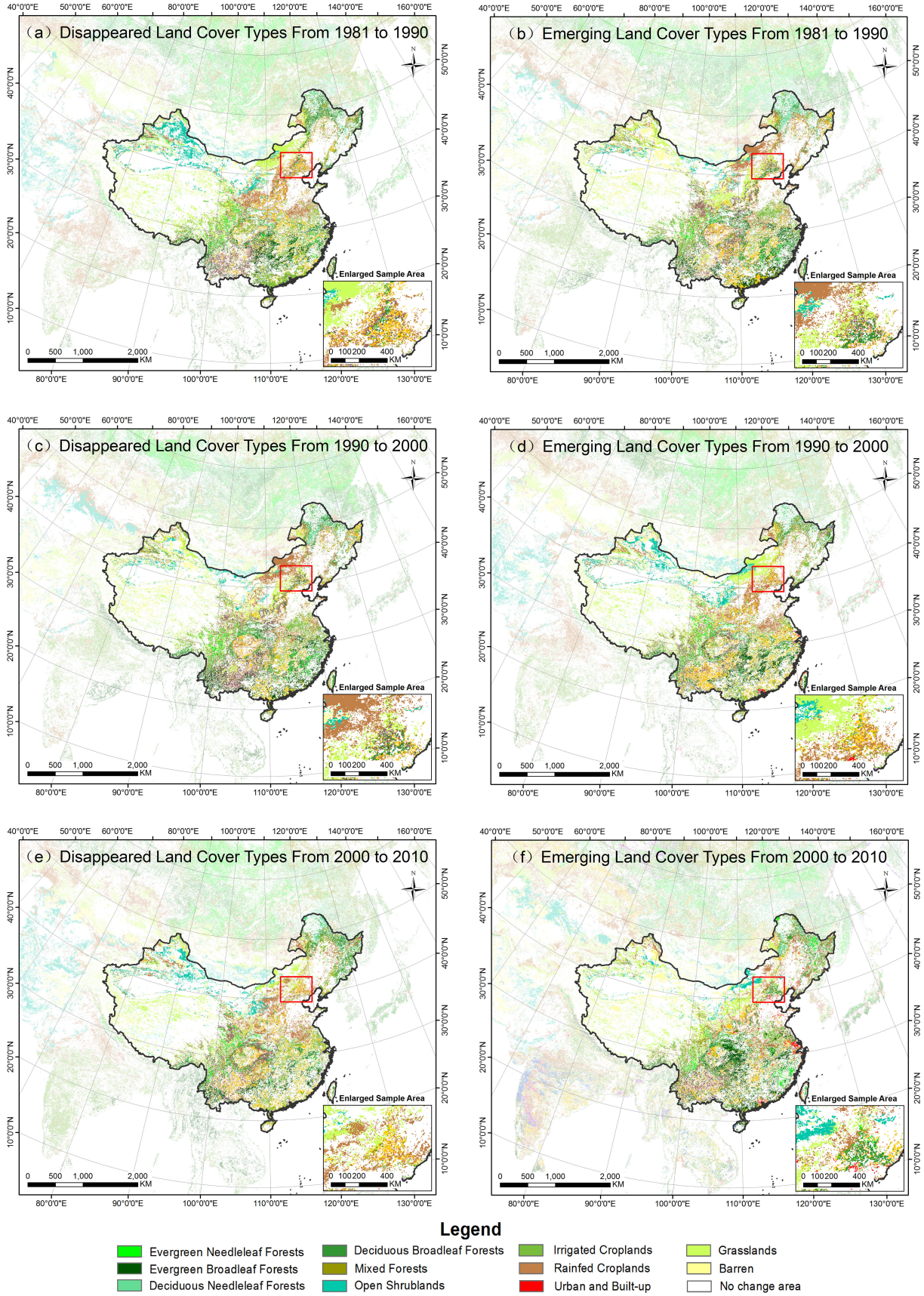

Fig. 5. Land cover change maps from (a, b) 1981–1990; (c, d) 1990–2000; and (e, f) 2000–2010. (a), (c), and (e) represent the disappeared land cover classes, while (b), (d), and (f) represent the emerging land cover classes within these three periods. The windows in the lower right-hand corner of the maps show an enlarged sample area around Hebei Province, denoted on the main maps by red rectangles.

rainfed cropland. Evergreen needleleaf forest was confused with the other four forest classes. Closed shrubland was also difficult to map since most misclassifications led to confusion between evergreen needleleaf forest and mixed forest.

B. Spatial Analysis of Land Cover Changes

The significant spatial land cover changes were mapped over the four periods.

1) As shown in Fig. 5(a) and (b), the land cover class with significant loss was open shrubland in the Junggar Basin from 1981 to 1990, where most of the open shrubland changed into grassland. Two classes of croplands in parts of northeast and eastern China mainly switched from one to the other, as did the forest (ID 1–5). Vast grassland in the Inner Mongolian Plateau converted into rainfed cropland. In the Loess Plateau, closed shrubland partially turned into grassland. Some forests in the Daxinganling diminished together with emerging cropland.
2) As shown in Fig. 5(c) and (d), less drastic changes occurred from 1990 to 2000. Partial changes occurred in most of eastern China, where forest changed into different forest or cropland. Similar transitions (from forest to cropland and from shrub to forest) increasingly occurred in southeast China. Along the Inner Mongolia Plateau, some closed shrubland changed into grassland and open shrubland. Degradation of rainfed cropland also emerged along the Northern China Plain. Meanwhile, some grassland changed into open shrubland along the junction of Kunlun Mountains and Tarim Basin.
3) As shown in Fig. 5(e) and (f), most changes occurred on the North China Plain, while the eastern China saw partial changes. Cropland/natural vegetation mosaic and cropland changed into grassland, mainly across central Inner Mongolia, southern Inner Mongolia, and the junction of Shaanxi and northwestern Xinjiang. Areas that changed from mosaic to broadleaf forest (e.g., the return of farmland to forest) were mainly situated in Southwest China.

Fig. 6 concludes the classes and amounts of areal change and ratio change for each period. As shown in Fig. 6(a), the most significantly areal changes occur in forest (ID 1–5), open shrubland (ID 7), grassland (ID 10), cropland/natural vegetation mosaic (ID 14), and cropland (ID 18, 19). There was no significant areal change in closed shrubland (ID 7), woody savanna (ID 8), savanna (ID 9), and tundra (ID 12). Among the other classes, permanent wetland (ID 11) fluctuated every decade. The open shrubland (ID 7) diminished from 1981 to 1990 before stabilizing from 1990 to 2000. More areas of open shrubland diminished from 2000 to 2010. As shown in Fig. 6(b), the evergreen needleleaf forest (ID 1) has the highest change ratio in the forest classes. The irrigated cropland (ID 18) has higher change ratio than rainfed cropland (ID 19) in every decade. The urban and built-up (ID 13) has the most remarkable gradual increase of change ratio. Comparatively, the grassland (ID 10), snow and ice (ID 15), and barren land (ID 16) changed less than 20%.

In order to further examine the land cover changes, the inter-transformation and changing with urban and built-up of three

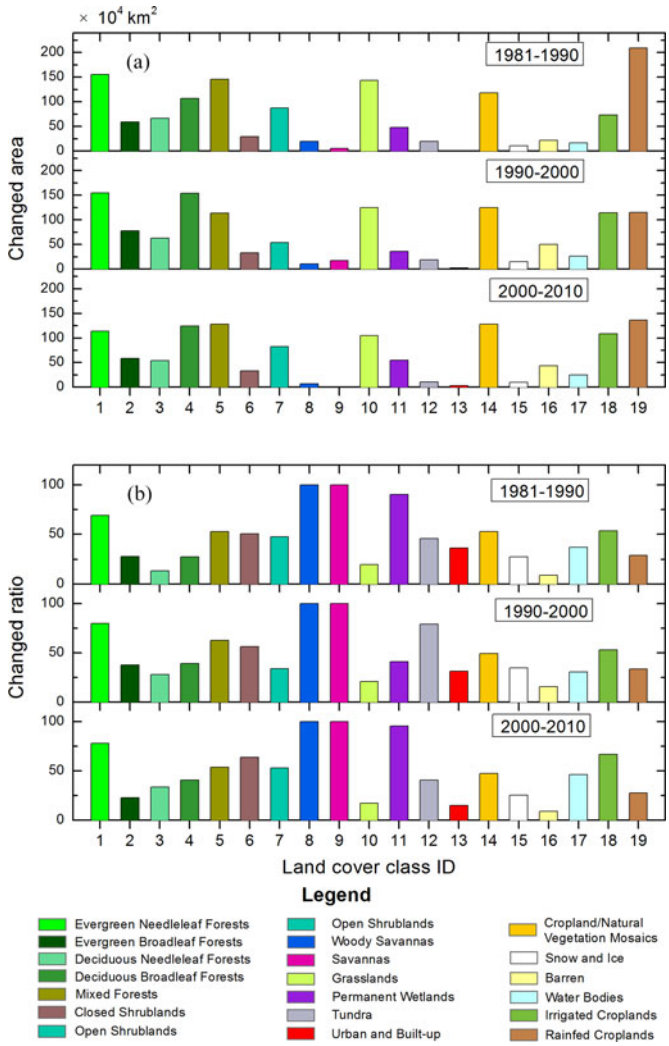

Fig. 6. Changed area (a) and ratio (b) of land cover classes for each period from 1981 to 2010.

typical land cover classes (i.e., cropland, grassland, and forest) were specialized investigated as follows. These changes were also verified using reference data extracted from higher-resolution dataset.

1) Cropland: The cropland area has experienced significant changes since 1981. We combined irrigated and rainfed cropland to observe the overall variation patterns. The total area of cropland underwent a decline, an increase, and then a decline from 1981 to 2010 but maintained an overall balance over the 30 years (see Fig. 7).

The total area of irrigated cropland showed a reduction trend from 1981 to 2010, including a decrease of 21% from 1981 to 1990, followed by a 9% increase from 1990 to 2000, and a further drop of 24% from 2000 to 2010 (see Fig. 8). In contrast, there was a continuous increase of 0.5%, 8%, and 3% for rainfed cropland in the three decades (see Fig. 9). The rate of increase was approximately equal to the inverse of the area change for irrigated cropland.

From 1981 to 1990, the land cover class with the most drastic changes to or from irrigated cropland was rainfed cropland,

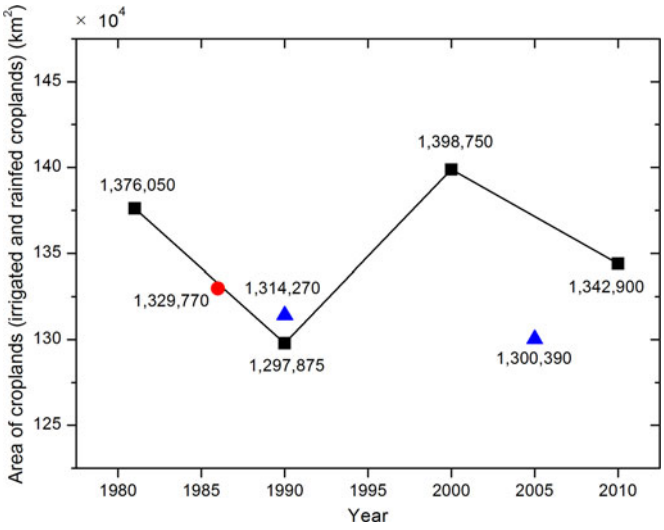

Fig. 7. Total area of cropland (including irrigated and rainfed cropland) in China from 1981 to 2010. The black squares represent cropland areas from the ChinaLC dataset. The red point represents the cropland area from the national cropland survey of 1986 [75]. The blue triangles represent cropland areas from the national land surveys of 1990 and 2005 [76].

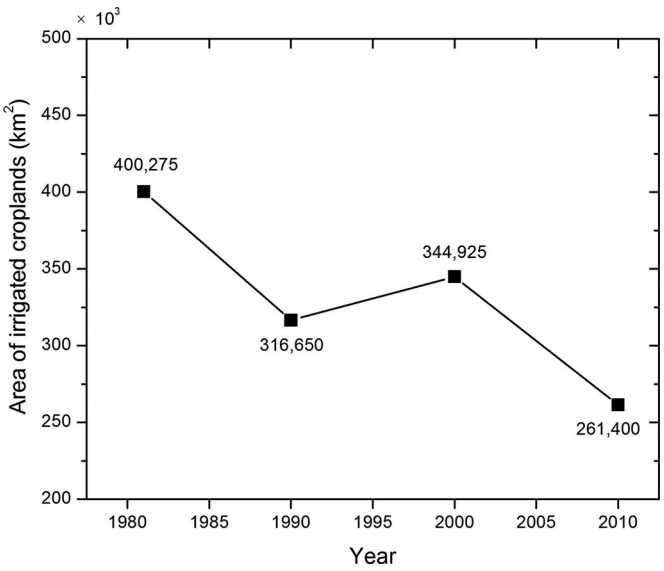

Fig. 8. Total area of irrigated cropland in China from 1981 to 2010.

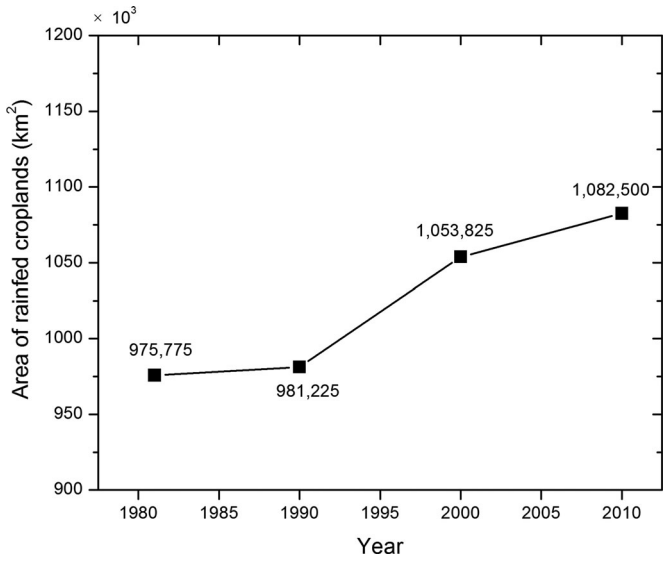

Fig. 9. Total area of rainfed cropland in China from 1981 to 2010.

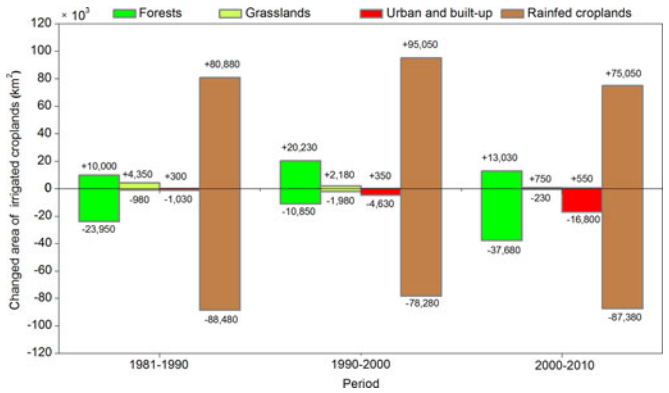

Fig. 10. Changed area between irrigated cropland and other land cover classes (bright green = forest; light green = grassland; red = urban and built-up land; brown = rainfed cropland) from 1981 to 1990, 1990 to 2000, and 2000 to 2010. "−" indicates areas in which irrigated cropland changed to other classes. "+" indicates areas in which other classes changed to irrigated cropland.

followed by forest (see Fig. 10). In total, there is a similar area of irrigated cropland changed to rainfed cropland as the reverse. More than twice the area of irrigated cropland changed into forest than the reverse. Grassland and urban and built-up areas showed small negative area values. From 1990 to 2000, less area changed from irrigated cropland to rainfed cropland than the reverse. More forest changed into irrigated cropland and more irrigated cropland changed into urban and built-up areas than during the 1980s. From 2000 to 2010, almost the same area changed between rainfed and irrigated cropland, accompanied by a greater area of irrigated cropland changed into forest than the reverse. Furthermore, the area of irrigated cropland that changed to urban and built-up areas was notable, reaching approximately four times the area during the 1990s [76].

Fig. 11 illustrates the changed area of rainfed cropland. The area of forest that changed to rainfed cropland was nearly double of which changed from rainfed cropland to forest from 1981 to 1990. Grassland shows the greatest change from 1990 to 2000. An increasing amount of grassland changed to rainfed cropland, while a decreasing area of rainfed cropland changed to grassland. The changed area between rainfed cropland and irrigated cropland remained stable, but the area of rainfed cropland that changed to forest was more than the forest area that changed to rainfed cropland. A significant area of urban and built-up land changed from 2000 to 2010, reflecting rapid urbanization during this period.

To verify the cropland changes revealed, we compared our results with those of different studies, with the following findings:

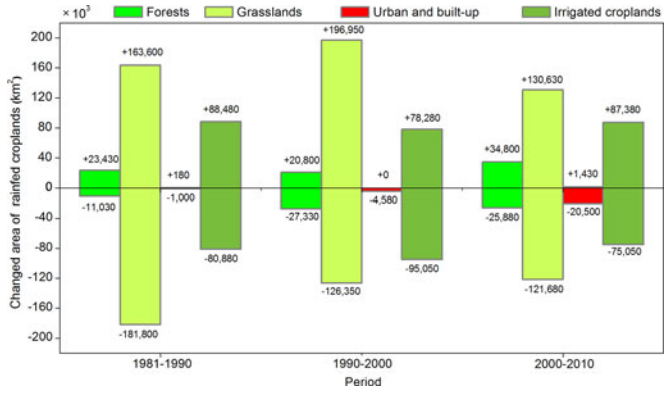

Fig. 11. Changed area between rainfed cropland and other land cover classes (bright green = forest; light green = grassland; red = urban and built-up land; deep green = irrigated cropland) from 1981 to 1990, 1990 to 2000, and 2000 to 2010. "−" indicates areas in which rainfed cropland changed to other classes. "+" indicates areas in which other class changed to rain-fed cropland.

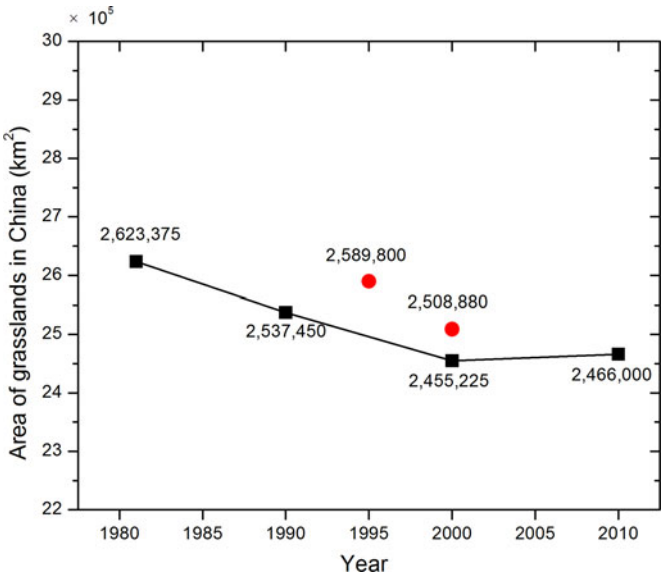

Fig. 12. Total area of grassland in China from 1981 to 2010. The black squares represent grassland areas in China from the ChinaLC dataset. The red points represent national grassland areas extracted from Landsat TM/ETM+ data in 1995 and 2000 [79].

1) the 1996 national land survey data and the second national land survey data show similar cropland areas in 1986 [75];
2) the statistical results from the Ministry of Land and Resource of China were referenced from 1996 to 2007. The result extracted from remote sensing images with 20–30 m spatial resolution (Landsat, CBERS, and HJ-1) was also used to indicate the crop area in 2000 [74]. These values fell between the overall cropland areas of the ChinaLC 1981 and 1990 dataset; and
3) the result of China's land use/cover datasets based on Landsat images indicated a raise and drop trend in cropland from 1990 to 2000 and from 2000 to 2010 [77]. These trends and increasing areas are all consistent with the variations observed in the ChinaLC dataset.

2) Grassland: Generally, the grassland area steadily decreased from 1981 to 2000, and then increased slightly from 2000 to 2010 (see Fig. 12), with a reduction rate of 6.05% from 1981 to 2010. However, grassland area slightly recovered from 2000 to 2010.

During the 30 years, the area of grassland that changed to urban and built-up land increased markedly (see Fig. 13). The changed area between grassland and forest varied greatly between different periods. More grassland changed into forest area than the reverse from 1981 to 1990 and from 2000 to 2010. In contrast, the area of grassland that changed to rainfed cropland was less than the area of rainfed cropland that changed to grassland from 1981 to 1990 and from 2000 to 2010.

Comparison of our results with other studies gave the following results:

1) the long-term trends of grassland biomass conducted using an NDVI time-series dataset from 1982 to 2003 indicated that grassland area increased in the mid-1980s, but then decreased until 1998 [78]; and
2) dynamic change in China's grassland, monitored using Landsat data [68], showed that the total grassland area decreased by approximately 80 000 km^2 from 1995 to 2000 (see Fig. 12).

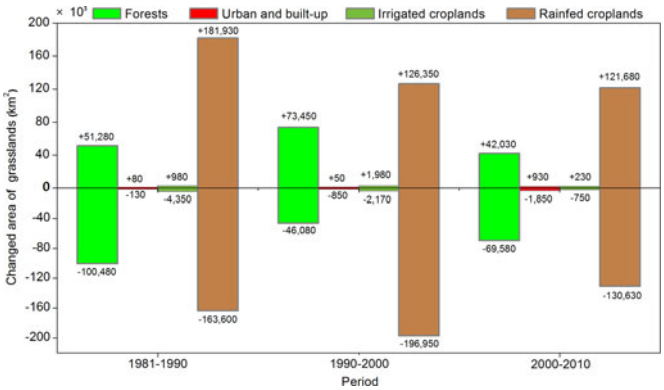

Fig. 13. Changed area between grassland and other land cover classes (bright green = forest; red = urban and built-up; deep green = irrigated cropland; brown = rainfed cropland) from 1981 to 1990, 1990 to 2000, and 2000 to 2010. "−" indicates areas in which grassland changed to other classes. "+" indicates areas in which other class changed to grassland.

3) Forest: We combined the five classes of forest (class ID 1–5) in order to observe the spatial–temporal changes in forest. The forest area of China increased first from 1981 to 1990, then sank to the lowest level at 2000, and then increased and reached the peak at 2010 (see Fig. 14).

The amount of forest area that changed to urban and built-up land increased rapidly from 1981 to 2010 (see Fig. 15). The change of forest area to and from rainfed cropland and irrigated cropland showed opposite patterns. Less forest area changed to rainfed cropland than to irrigated cropland from 1981 to 1990 and from 2000 to 2010.

Previous research result from the land-use/cover data set of national resources and environment database illustrated the overall forest area, and showed an increase from 1985 to 1995 [80]. From 1995 to 2000, the overall area of forest decreased, with shrubland and sparse forest lost, although there was also an

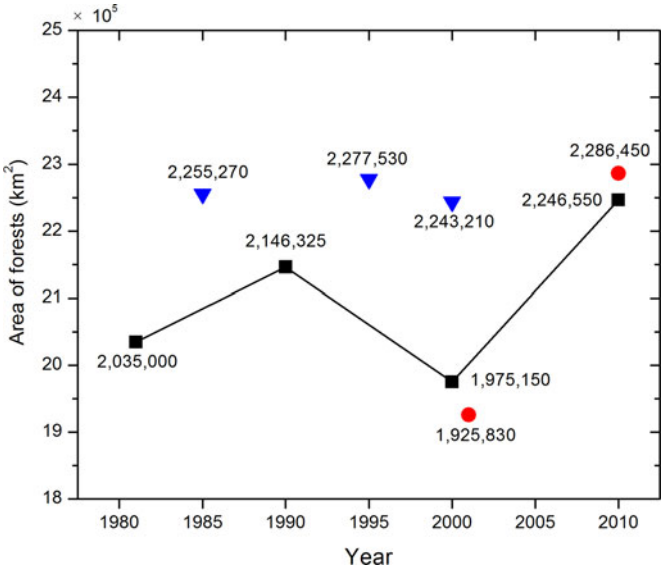

Fig. 14. Total area of forest in China from 1981 to 2010. Black squares represent forest areas from the ChinaLC dataset. The red points represent forest areas extracted from the MCD12Q1 products in 2001 and 2010 [71]. The blue triangles represent the forest areas extracted from Landsat TM/ETM+ data in 1985, 1995, and 2000 [69].

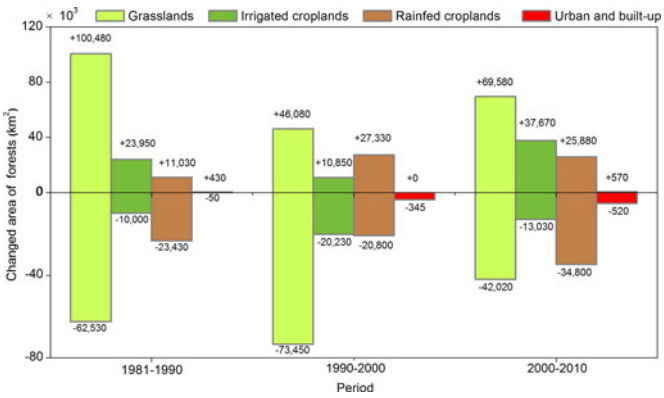

Fig. 15. Changed area between forest and other land cover classes (bright green = grassland; deep green = irrigated cropland; brown = rainfed cropland; red = urban and built-up) from 1981 to 1990, 1990 to 2000, and 2000 to 2010. "−" indicates areas in which forest changed to other classes. "+" indicates areas in which other class changed to forest.

increase in dense forest cover. The observed dense forest cover decrease from 1985 to 1995 was consistent with our result since the definition of forest class in the ChinaLC dataset did not include the shrubland class. Excluding the net decrease of sparse forest and shrubland, the remaining net increase in dense forest also agreed with our results of forest changes from 2000 to 2010.

Other studies incorporated MCD12Q1 and NDVI data in order to obtain the NDVI time-series for 500-m resolution forest coverage calculations from 2001 to 2011. The results indicated that the forests distribution in China expanded slowly each year between 2002 and 2011. New forest rose from 10% in 2002 to 44.2% in 2011 [81]. These trends are consistent with our 2000–2010 observations from the ChinaLC dataset. In summary, the validation data were broadly consistent with those of the ChinaLC dataset.

V. Discussion

A. Issues Related to Sample Selection

A collection of adequate and representative training and validation samples is the key factor influencing land cover classification. In this study, multisource reference data were integrated to collect samples by visual interpretation and collaborative decisions from experts, and to obtain a representative and valuable decadal sample dataset of the 30 years. At present, GE has the largest collection of panoramic images for browsing purposes, which are readily available, time-stamped, and useful when lacking valid visual interpretation of high-resolution images, as well as for double verification purposes. The samples used for producing current land cover datasets are far from abundant and not totally uniformly distributed over China. This case could also illustrate the low accuracy in some areas of our datasets. Attempts should be made in the future to use international and professional crowdsourcing to collect samples with well representation in both geographical distribution and product validation for land cover classes.

B. Metric Determination and Dimension Reduction

Until now, reflectance data, VIs, and DEM are still the main data source for land cover mapping at global scale in consideration of their responses to different land cover classes. The reflectance data may be useful for separating classes with different characteristics but not for separating canopy closures. The VIs are essential for land cover classification. Separation would be easier using the amplitude of NDVI or EVI. Other environmental information, such as climate and topography data, could be used as additional features to improve classification accuracy on a large scale. Moreover, the metrics were mainly designed based on the vegetation phenology, which resulted in the classes of grassland, forest, and cropland having better classification accuracy. However, the representative metrics for classes with mixed components such as wetland, mixed forest, and cropland/natural vegetation mosaic have not been determined yet and more effective metrics that would help the separation are needed.

Besides, the data volume, cross validation accuracy, and running time increased simultaneously as the metrics number increased. We found that the dimension reduction by PCA would remarkably decrease the running time but the cross validation accuracy would also decrease slightly. We selected the metrics without processing by PCA in order to achieve an approximately 2% increase in cross validation accuracy. However, if producing monthly or seasonal products, the running time or repeatability would be considered as a more important factor. Thus, the selection of metrics should consider both accuracy and efficiency of land cover dataset production.

C. Efforts Related to the Improvement of Accuracy

Multiple methods were integrated into the proposed classification procedure. The thematic information extraction was used to identify urban and built-up areas. The SVM was selected for its ability in dealing with large number of alternative metrics and

small number of training samples. The optimal classification parameters were obtained by the cross-validation method, so that the classifier was robust, consistent, and repeatable in terms of reference data error and heterogeneous classes. The land cover classes with a small number of samples (e.g., wetlands, tundra, closed shrubland, and open shrubland) were classified with acceptable accuracies and showed reasonable patterns. The scarcity of typical land cover classes in China (e.g., savanna and woody savanna) may be a reason for the relative low accuracy.

Moreover, to produce the multiphase datasets, improvements were made by using the relative reflectance correction to adjust consistency in the four phases. The spatial consistency of the ChinaLC dataset validated the effectiveness of the correction. Even so, almost every land cover class showed some disturbance during the study period, with these disturbances partially explained by the misclassification of some large area land cover fluctuations (e.g., cropland/natural vegetation mosaic). The limited number of representative samples was also responsible for unusual fluctuations. The lowest overall accuracy of the map in 1981, which can be explained by the deficiency of comprehensive samples than other phases, highlights the importance of sample representation in land cover classification. By comparing the overall accuracy with other global large-scale land cover datasets, we see clear increases in accuracy with the ChinaLC dataset.

D. Possible Drivers for the Land Cover Changes

The possible drivers that explained the land cover changes can be analyzed in two phases. From 1980 to 2000, there was a continuous transform from naturalized classes (e.g., grassland, forest, and rainfed cropland) to human disturbed classes (e.g., irrigated cropland, urban and built-up). This can be explained as an integrated result of 1) land degradation, cropland reclamation, and deforestation; and 2) increasing food and land demands driven by rapid population growth and fast urbanization. However, from 2000 to 2010, almost the same area changed between rainfed and irrigated cropland, but a greater area of irrigated cropland changed into forest than the reverse. The grassland area also recovered slightly. This may result from

1) the national "Grain for Green" project in 1999, designed for the sake of ecological conservation;
2) the national "Return Farmland to Forest" project, designed to fulfill a huge demand for wood and industrial development; and
3) ecological restoration programs implemented by the government to control grassland degradation.

By the analysis of the above-mentioned drivers for the transformation, we found that the national eco-environmental policies indeed reduced the disappearance rate of original cropland, and excessive reclamation resulted in the transition of more grassland and forest into cropland especially from 2000; generally, human activity (e.g., urbanization) is the major cause of accelerated landscape changes.

E. Applications of the ChinaLC Dataset

The ChinaLC dataset has been proved to be valid, reasonable, and reliable after being used as a crucial and fundamental input parameter in many studies, including on aerosol transport [82], precipitation simulations [83], changes in temperature amplitude, and climate variability [84], [85] in eastern Asia or China. Human influences on seasonal temperature changes in mid- to high-latitude areas have also been analyzed [86]. Considering these practical studies, there would be more applications of the ChinaLC dataset for the future. Further investigations should include more detailed analyses of the dynamics related to detrimental climate events, land policy, and the physical environment of China in order to deepen our understanding of land cover changes in a socio-historical context.

VI. Conclusion

The aim of this study is to design a multitemporal classification chain which enables a standardized, repeatable, and temporally transferable derivation of land cover information for national land cover change analysis. The proposed land cover classification approach was innovative in the following aspects:

1) the 30-year decadal maps were produced at 5-km resolution with improved precision and consistency for the different phases;
2) the multisource reference data were integrated for visual interpretation, obtaining a representative decadal sample dataset of 30 years;
3) considering the response to different land cover classes and the factors from terrain, the final metrics with the highest cross validation accuracy were selected from the alternative metric combinations;
4) for robust, consistent, and repeatable land cover classification in terms of reference data error and heterogeneous classes, the optimal classification parameters were obtained by the cross-validation method; and
5) the improvements were conducted by relative reflectance correction to adjust consistency for reflectance and VIs in the four phases.

Analysis results from the ChinaLC dataset indicated that some land cover classes (e.g., grassland and forest) became fragmented and fragile in certain areas and the patterns of change differed across the 30 years. Vast areas of shrubland diminished and grassland emerged during the first decade while cropland displaced forest and grassland. The decadal net loss of forest, shrubland, and grassland was significantly greater than the net loss of cropland. Subsequent analysis showed that this pattern continued into the 2000s. Although national eco-environmental policies reduced the rate of change of cropland to grassland and forest area, excessive reclamation resulted in more grassland and forest area changing into cropland. The eco-environment in this region is fragile, and extensive human activities may be the most important reason for accelerated landscape change, some of which is difficult to restore (e.g., the evolution to barren).

Acknowledgment

The authors would like to thank the following colleagues who provided valuable suggestions for this work: Prof. C. Fu, Prof. W. Guo, Assoc. Prof. S. Wang, Prof. A. Ding, Prof. Y. Zhou, and Assoc. Prof. X. Jin of the Nanjing University, Prof. X. Cui, Prof. J. Chen, and Prof. W. Zhu of the Beijing Normal University, and

Porf. G. Jia and Prof. D. Zhao of the Institute of Atmospheric Physics, Chinese Academy of Sciences. The authors appreciate thoughtful reviews by anonymous referees.

REFERENCES

[1] A. Di Gregorio and L. J. Jansen, *Land Cover Classification System (LCCS): Classification Concepts and User Manual for Software Version 1.0*. Rome, Italy: Food Agriculture Org., 2000.

[2] R. DeFries, M. Hansen, and J. Townshend, "Global discrimination of land cover types from metrics derived from AVHRR pathfinder data," *Remote Sens. Environ.*, vol. 54, no. 95, pp. 209–222, Dec. 1995.

[3] J. W. Yan *et al.*, "Changes in the land surface energy budget in eastern China over the past three decades: Contributions of land-cover change and climate change," *J. Clim.*, vol. 27, no. 24, pp. 9233–9252, 2014.

[4] Z. G. Bai and D. Dent, "Recent land degradation and improvement in China," *AmBio*, vol. 38, no. 3, pp. 150–156, 2009.

[5] M. C. Hansen, R. S. DeFries, R. G. John, and R. Sohlberg, "Global land cover classification at 1 km spatial resolution using a classification tree approach," *Int. J. Remote Sens.*, vol. 21, no. 6, pp. 1331–1364, Nov. 2000.

[6] J. Cihlar, "Land cover mapping of large areas from satellites: Status and research priorities," *Int. J. Remote Sens.*, vol. 21, no. 6, pp. 1093–1114, Nov. 2010.

[7] T. R. Loveland, B. C. Reed, J. F. Brown, D. O. Ohlen, Z. Zhu, and J. W. Merchant, "Development of a global land cover characteristics database and IGBP DISCover from 1 km AVHRR data," *Int. J. Remote Sens.*, vol. 21, no. 6, pp. 1303–1330, Nov. 2000.

[8] E. Bartholomé and A. S. Belward, "GLC2000: A new approach to global land cover mapping from earth observation data," *Int. J. Remote Sens.*, vol. 26, no. 9, pp. 1959–1977, May 2005.

[9] M. A. Friedl, D. K. McIver, J. C. F. Hodges, X. Y. Zhang, D. A. Muchoney, and H. C. E. Strahler, "Global land cover mapping from MODIS: Algorithms and early results," *Remote Sens. Environ.*, vol. 83, no. 1, pp. 287–302, Nov. 2002.

[10] M. A. Friedl *et al.*, "MODIS collection 5 global land cover: Algorithm refinements and characterization of new datasets," *Remote Sens. Environ.*, vol. 114, no. 1, pp. 168–182, Jan. 2010.

[11] R. Tateishi, B. Uriyangqai, and H. Al-Bilbisi, "Production of global land cover data–GLCNMO," *Int. J. Digit. Earth*, vol. 4, no. 1, pp. 22–49, Jan. 2011.

[12] S. Bontemps, P. Defourny, E. Bogaert, O. Arino, V. Kalogirou, and J. Perez, "GLOBCOVER 2009–Products description and validation report," Eur. Space Agency, Paris, France, (2011). [Online]. Available: http://due.esrin.esa.int/files/GLOBCOVER2009_Validation_Report_2.2.pdf

[13] P. Defourny *et al.*, "Land cover CCI," in *Product User Guide Version 2*. Paris, France: Eur. Space Agency, 2014.

[14] P. Gong, J. Wang, Y. Yu, Y. Zhao, L. Zhao, and Z. Liang, "Finer resolution observation and monitoring of global land cover: First mapping results with Landsat TM and ETM+ data," *Int. J. Remote Sens.*, vol. 34, no. 7, pp. 2607–2654, Dec. 2012.

[15] J. Chen and A. Liao, "Global land cover mapping at 30 m resolution: A POK-based operational approach," *ISPRS J. Photogramm.*, vol. 103, pp. 7–27, May 2015.

[16] J. Scepan, "Thematic validation of high-resolution global land-cover data sets," *Photogramm. Eng. Remote Sens.*, vol. 65, pp. 1051–1060, 1999.

[17] Y. H. Ran, X. Li, and L. Lu, "Evaluation of four remote sensing based land cover products over China," *Int. J. Remote Sens.*, vol. 31, pp. 391–401, 2010.

[18] P. Mayaux *et al.*, "Validation of the global land cover 2000 map," *IEEE Trans. Geosci. Remote Sens.*, vol. 44, no. 7, pp. 1728–1739, Jul. 2006.

[19] M. A. Friedl *et al.*, "MODIS collection 5 global land cover: Algorithm refinements and characterization of new datasets," *Remote Sens. Environ.*, vol. 114, pp. 168–182, 2010.

[20] R. Tateishi, N. T. Hoan, T. Kobayashi, B. Alsaaideh, G. Tana, and D. X. Phong, "Production of global land cover data–GLCNMO2008," *J. Geography Geol.*, vol. 6, no. 3, pp. 99–123, 2014.

[21] P. Bicheron *et al.*, "Globcover—Products description and validation report," Eur. Space Agency, Paris, France, (2008). [Online]. Available: http://postel.obs-mip.fr/IMG/pdf/GLOBCOVER_Products_Description_Validation_Report_I2.1.pdf

[22] N. E. Tsendbazar, S. De Bruin, and M. Herold, "Assessing global land cover reference datasets for different user communities," *ISPRS J. Photogramm.*, vol. 103, pp. 93–114, 2015.

[23] P. Gong *et al.*, "Finer resolution observation and monitoring of global land cover: First mapping results with Landsat TM and ETM+ data," *Int. J. Remote Sens.*, vol. 34, no. 7, pp. 2607–2654, 2013.

[24] J. Chen *et al.*, "Global land cover mapping at 30 m resolution: A POK-based operational approach," *ISPRS J. Photogramm.*, vol. 103, pp. 7–27, 2015.

[25] N. Zhang and R. Tateishi, "Integrated use of existing global land cover datasets for producing a new global land cover dataset with a higher accuracy: A case study in Eurasia," *Adv. Remote Sens.*, vol. 2, no. 4, pp. 365–372, 2013.

[26] G. Han, J. Chen, and C. He, "A web-based system for supporting global land cover data production," *ISPRS J. Photogramm. Remote Sens.*, vol. 103, pp. 66–80, 2015.

[27] Y. Rao, X. Zhu, and J. Chen, "An improved method for producing high spatial-resolution NDVI time series datasets with multi-temporal MODIS NDVI data and Landsat TM/ETM+ images," *Remote Sens.*, vol. 7, no. 6, pp. 7865–7891, 2015.

[28] D. Lu and Q. Weng, "A survey of image classification methods and techniques for improving classification performance," *Int. J. Remote Sens.*, vol. 28, no. 5, pp. 823–870, Mar. 2007.

[29] G. M. Foody, "Status of land cover classification accuracy assessment," *Remote Sens. Environ.*, vol. 80, pp. 185–201, 2002.

[30] J. Townshend, C. Justice, W. Li, C. Gurney, and J. McManus, "Global land cover classification by remote sensing: Present capabilities and future possibilities," *Remote Sens. Environ.*, vol. 35, pp. 243–255, 1991.

[31] J. F. Brown, T. R. Loveland, D. O. Ohlen, and Z. L. Zhu, "The global land-cover characteristics database: The users' perspective," *Photogramm. Eng. Remote Sens.*, vol. 65, pp. 1069–1074, 1999.

[32] S. Fritz and L. See, "Identifying and quantifying uncertainty and spatial disagreement in the comparison of global land cover for different applications," *Global Change Biol.*, vol. 14, pp. 1057–1075, 2008.

[33] R. Congalton, J. Gu, K. Yadav, P. Thenkabail, and M. Ozdogan, "Global land cover mapping: A review and uncertainty analysis," *Remote Sens.*, vol. 6, pp. 12070–12093, 2014.

[34] C. Giri, Z. Zhu, and B. Reed, "A comparative analysis of the global land cover 2000 and MODIS land cover data sets," *Remote Sens. Environ.*, vol. 94, pp. 123–132, 2005.

[35] P. Gong, L. Yu, and C. Li, "A new research paradigm for global land cover mapping," *Ann. GIS*, vol. 22, pp. 1–16, 2016.

[36] C. Giri, Z. Zhu, and B. Reed, "A comparative analysis of the global land cover 2000 and MODIS land cover data sets," *Remote Sens. Environ.*, vol. 94, no. 1, pp. 123–132, Jan. 2005.

[37] E. Vintrou, M. Soumaré, and S. Bernard, "Mapping fragmented agricultural systems in the Sudano–Sahelian environments of Africa using random forest and ensemble metrics of coarse resolution MODIS imagery," *Photogramm. Eng. Remote Sens.*, vol. 78, no. 8, pp. 839–848, Aug. 2012.

[38] I. McCallum, M. Obersteiner, S. Nilsson, and A. Shvidenko, "A spatial comparison of four satellite derived 1 km global land cover datasets," *IEEE J. Sel. Topic Appl. Earth Observ. Remote Sens.*, vol. 8, no. 4, pp. 246–255, Dec. 2006.

[39] Y. Yang, P. Xiao, X. Feng, H. Li, X. Chang, and W. Feng, "Comparison and assessment of large-scale land cover datasets in China and adjacent regions," *J. Remote Sens.*, vol. 18, no. 2, pp. 453–475, 2014 (in Chinese).

[40] G. M. Foody, "Status of land cover classification accuracy assessment," *Remote Sens. Environ.*, vol. 80, pp. 185–201, 2002.

[41] J. Pedelty *et al.*, "Generating a long-term land data record from the AVHRR and MODIS instruments," in *Proc. IEEE Int. Geosci. Remote Sens. Symp.*, Jul. 2007, pp. 1021–1025.

[42] L. Wang, P. Xiao, X. Feng, H. Li, W. Zhang, and J. Lin, "Effective compositing method to produce cloud-free AVHRR Image," *IEEE Geosci. Remote Sens.*, vol. 11, no. 1, pp. 328–332, Jan. 2014.

[43] J. Llf, M. N. Jaarsma, and L. Etmvander, "Integrating topographic data with remote sensing for land-cover classification," *Photogramm. Eng. Remote Sens.*, vol. 56, pp. 1503–1506, 1990.

[44] T. Tachikawa, H. Masami Hato, K. Manabu, and I. Akira, "Characteristics of ASTER GDEM version 2," in *Proc. IEEE Int. Geosci. Remote Sens. Symp.*, 2011, pp. 3657–3660.

[45] X. Cao, J. Chen, H. Imura, and O. Higashi, "A SVM-based method to extract urban areas from DMSP-OLS and SPOT VGT data," *Remote Sens. Environ.*, vol. 113, no. 10, pp. 2205–2209, Oct. 2009.

[46] X. Y. Hou, *The Vegetation Map of China (1: 4 000 000)*. Beijing, China: Science, 1982 (in chinese).

[47] X. Y. Hou, *The Vegetation Atlas of China (1: 1 000 000)*. Beijing, China: Science, 2001 (in chinese).

[48] A. Dorais and J. Cardille, "Strategies for incorporating high-resolution Google Earth databases to guide and validate classifications: Understanding deforestation in Borneo," *Remote Sens.*, vol. 3, no. 6, pp. 1157–1176, 2011.
[49] A. S. Belward, "The IGBP-DIS global 1-km land-cover data set DISCover: A project overview," *Photogramm. Eng. Remote Sens.*, vol. 65, no. 9, pp. 1013–1020, 1996.
[50] S. W. Running, R. L. Thomas, and L. P. Lars, "A vegetation classification logic based on remote sensing for use in global biogeochemical models," *AmBio*, vol. 23, no. 1, pp. 77–81, 1994.
[51] Y. Liu, J. Wang, and L. Guo, "The spatial-temporal changes of grain production and arable land in China," *Sci. Agricultura Sinica*, vol. 42, pp. 4269–4274, 2009 (in Chinese).
[52] J. Bruinsma, *World Agriculture: Towards 2015/2030: An FAO Perspective*. London, U.K.: Earthscan, 2003, pp. 124–148.
[53] L. Bounoua, R. DeFries, and G. J. Collatz, "Effects of land cover conversion on surface climate," *Clim. Change*, vol. 52, no. 1, pp. 29–64, 2002.
[54] J. Schneider, G. Grosse, and D. Wagner, "Land cover classification of tundra environments in the arctic lena Delta based on landsat 7 ETM+ data and its application for upscaling of methane emissions," *Remote Sens. Environ.*, vol. 113, no. 2, pp. 380–391, Feb. 2009.
[55] R. S. Defries and J. R. G. Townshend, "NDVI-derived land cover classification at a global scale," *Int. J. Remote Sens.*, vol. 15, no. 17, pp. 3567–3586, 1994.
[56] R. Defries, M. Hansen, and J. Townshend, "Global discrimination of land cover types from metrics derived from AVHRR pathfinder data," *Remote Sens. Environ.*, vol. 54, no. 95, pp. 209–222, 1995.
[57] Y. Gao, J. F. Mas, and A. Navarrete, "The improvement of an object-oriented classification using multi-temporal MODIS EVI satellite data," *Int. J. Digit. Earth*, vol. 2, no. 3, pp. 219–236, 2009.
[58] R. S. De Fries, M. Hansen, J. R. G. Townshend, and R. Sohlberg, "Global land cover classifications at 8 km spatial resolution: The use of training data derived from Landsat imagery in decision tree classifiers," *Int. J. Remote Sens.*, vol. 19, no. 16, pp. 3141–3168, 1998.
[59] E. F. Lambin and D. Ehrlich, "The surface temperature-vegetation index space for land cover and land-cover change analysis," *Int. J. Remote Sens.*, vol. 17, no. 3, pp. 463–487, 1996.
[60] D. Lloyd, "A phenological classification of terrestrial vegetation cover using shortwave vegetation index imagery," *Int. J. Remote Sens.*, vol. 11, no. 12, pp. 2269–2279, 1990.
[61] W. J. Leeuwen and D. Van, "Phenological characterization of desert sky island vegetation communities with remotely sensed and climate time series data," *Remote Sens.*, vol. 2, no. 2, pp. 388–415, 2010.
[62] A. Fahsi, T. Tsegaye, W. Tadesse, and T. Coleman, "Incorporation of digital elevation models with Landsat-TM data to improve land cover classification accuracy," *Forest Ecol. Manage.*, vol. 128, nos. s1–s2, pp. 57–64, 2000.
[63] P. K. Srivastava, D. Han, M. A. Rico-Ramirez, M. Bray, and T. Islam, "Selection of classification techniques for land use/land cover change investigation," *Adv. Space Res.*, vol. 50, no. 9, pp. 1250–1265, Nov. 2012.
[64] J. K. Otukei and T. Blaschke, "Land cover change assessment using decision trees, support vector machines and maximum likelihood classification algorithms," *Int. J. Appl. Earth Observ. Geoinf.*, vol. 12, pp. S27–S31, Feb. 2010.
[65] S. Yang and R. S. Lunetta, "Comparison of support vector machine, neural network, and CART algorithms for the land-cover classification using limited training data points," *ISPRS J. Photogramm.*, vol. 70, pp. 78–87, Jun. 2012.
[66] G. M. Foody, A. Mathur, C. Sanchez-Hernandez, and D. S. Boyd, "Training set size requirements for the classification of a specific class," *Remote Sens. Environ.*, vol. 104, no. 1, pp. 1–14, Sep. 2006.
[67] G. M. Foody and A. Mathur, "The use of small training sets containing mixed pixels for accurate hard image classification: Training on mixed spectral responses for classification by a SVM," *Remote Sens. Environ.*, vol. 103, no. 2, pp. 179–189, Jul. 2006.
[68] M. P. Ferreira, M. Zortea, D. C. Zanotta, Y. E. Shimabukuro, and C. R. Filho, "Mapping tree species in tropical seasonal semi-deciduous forest with hyperspectral and multispectral data," *Remote Sens. Environ.*, vol. 179, pp. 66–78, Jun. 2016.
[69] C. Alcantara, T. Kuemmerle, A. V. Prishchepov, and V. C. Radeloff, "Mapping abandoned agriculture with multi-temporal MODIS satellite data," *Remote Sens. Environ.*, vol. 124, pp. 334–347, Sep. 2012.
[70] C. Chang and C. Lin, "LIBSVM: A library for support vector machines," *ACM Trans. Intell. Syst. Technol.*, vol. 2, pp. 1–27, 2011.
[71] C. W. Hsu, C. C. Chang, and C. J. Lin, "A practical guide to support vector classification," Dept. Comput. Sci. Inf. Eng., Univ. Nat., Taiwan, Taipei, Tech. Rep., pp. 1–12, (2003). [Online]. Available: https://www.csie.ntu.edu.tw/˜cjlin/papers/guide/guide.pdf
[72] P. Zhang, X. Yu, and Z. Liu, "A study on relative radiometric correction of multitemporal remote sensing images," *J. Remote Sens.*, vol. 10, no. 3, pp. 330–344, 2006 (in Chinese).
[73] P. Xiao, X. Wang, X. Feng, X. Zhang, and Y. Yang, "Detecting China's urban expansion over the past three decades using nighttime light data," *IEEE J. Sel. Topic Appl. Earth Observ. Remote Sens.*, vol. 7, no. 10, pp. 4095–4106, Oct. 2014.
[74] P. Xiao, H. Li, Y. Yang, L. Wang, and X. Wang, "Land-use changes in China during the past 30 years," in Land-Use Changes in China. Singapore: World Scientific, Aug. 2015, pp. 11–49.
[75] Y. Lu and Y. Cui, "A study on the temporal-spatial changes and its influencing factors of China's arable land during 1986–2007," *J. Xinyang Normal Univ.*, vol. 23, no. 2, pp. 245–249, Feb. 2010 (in Chinese)
[76] J. Liu, M. Liu, and H. Tian, "Spatial and temporal patterns of China's cropland during 1990–2000: An analysis based on Landsat TM data," *Remote Sens. Environ.*, vol. 98, no. 4, pp. 442–456, Oct. 2005.
[77] H. Huijuan and X. Shi, "Spatio-temporal characteristics of land cover changes in China during 1990–2010," *J. Geo-Inf. Sci.*, vol. 11, pp. 1323–1332, 2015.
[78] Y. Zou, X. Zhao, and Z. Zhang, "An analysis of dynamic changes of China's grassland on the basis of RS and GIS," *Remote Sens. Land Resour.*, vol. 14, no. 1, pp. 29–33, 2002 (in Chinese).
[79] L. Xiu, Q. Feng, T. Liang, and J. Ren, "Spatial and temporal distribution of grassland and human occupancy condition in China from 2001 to 2009," *J. Hortic. Sci.*, vol. 31, pp. 66–74, Jan. 2014.
[80] X. Xu, J. Liu, D. Zhuang, and S. Zhang, "Spatial-temporal characteristics and driving forces of woodland resource changes in China," *J. Beijing Forestry Univ.*, vol. 26, no. 1, pp. 41–46, Jan. 2004 (in Chinese).
[81] R. Nemani and S. W. Running, "Satellite monitoring of global land cover changes and their impact on climate," *Clim. Change*, vol. 31, no. 2, pp. 395–413, 1995.
[82] J. Wu, J. Guo, and D. Zhao, "Characteristics of aerosol transport and distribution in East Asia," *Atmos. Res.*, vol. 132–133, pp. 185–198, Oct. 2013.
[83] D. Zhao, "Performance of regional integrated environment modeling system (RIEMS) in precipitation simulations over East Asia," *Clim. Dyn.*, vol. 40, no. 7, pp. 1767–1787, Apr. 2013.
[84] C. Qian, C. Fu, and Z. Wu, "Changes in the amplitude of the temperature annual cycle in China and their implication for climate change research," *J. Clim.*, vol. 24, no. 20, pp. 5292–5302, Oct. 2011.
[85] H. Chen, X. Li, and W. Hua, "Numerical simulation of the impact of land use/land cover change over China on regional climates during the last 20 years," *Chin. J. Atmos. Sci.*, vol. 39, no. 2, pp. 357–369, 2015 (in Chinese).
[86] C. Qian and X. Zhang, "Human influences on changes in the temperature seasonality in mid-to-high latitude land areas," *J. Clim.*, vol. 28, no. 15, pp. 5908–5921, Aug. 2015.

Haixing Li was born in Nanjing, Jiangsu, China, in 1985. She received the B.S. degree in geographical information system from the Nanjing University of Technology, Nanjing, China, in 2008. She is currently working toward the Ph.D. degree in cartography and geographical information system at Nanjing University, Nanjing, China.

She is the author of three articles. Her research interests include land use and land cover change and remote sensing of snow.

Pengfeng Xiao (M'13) was born in Ningxiang, Hunan, China, in 1979. He received the B.S. degree in land resource management from the Hunan Normal University, Changsha, China, in 2004, and the Ph.D. degree in cartography and geographical information system from Nanjing University, Nanjing, China, in 2007.

From 2007 to 2009, he was a Lecturer in the Department of Geographic Information Science, Nanjing University, where he has been an Associate Professor since 2010. He is the author of two books and more than 50 articles. His research interests include remote sensing image segmentation, land use and land cover change, and remote sensing of snow.

Xuezhi Feng was born in Dingxi, Gansu, China, in 1953. He received the B.S. degree in cartography from Nanjing University, Nanjing, China, in 1979.

From 1980 to 1981, he was a Lecturer in the Department of Geography, Nanjing University. He was then employed by the Lanzhou Institute of Glaciology and Cryopedology, Chinese Academy of Sciences, as an Assistant Professor from 1981 to 1990, as an Associate Professor from 1990 to 1994, as a Professor from 1994 to 1997. Since 1997, he has been a Professor in the Department of Geographic Information Science, Nanjing University. He is the author of four books and more than 200 articles. His research interests include remote sensing of snow and remote sensing image processing.

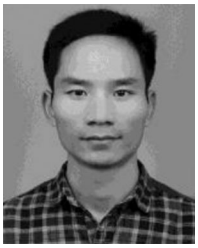

Yongke Yang was born in Luoyang, Henan, China, in 1987. He received the B.S. degree in geographical information system from Xuchang University, Xuchang, China, in 2011, and the M.S. degree in 2014 in cartography and geographical information system from Nanjing University, Nanjing, China, where he is currently working toward the Ph.D. degree in cartography and geographical information system.

He is the author of three articles. His research interests include remote sensing of snow and land use and land cover change.

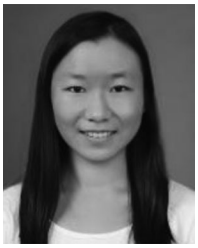

Lingxiao Wang was born in Chuzhou, Anhui, China, in 1988. She received the B.S. degree in geographical information system from the South China Normal University, Guangzhou, China, in 2009, and the M.S degree in cartography and geographical information system from Nanjing University, Nanjing, China, in 2012. She is currently working toward the Ph.D. degree in physical geography and remote sensing at the University of Munich, Munich, Germany.

She is the author of one article. Her research interests include remote sensing of permafrost landscape and ground surface deformation along with environment modeling.

Wenbo Zhang was born in Jilin, Jilin, China, in 1987. He received the B.S. degree in geographical information system and the M.S. degree in cartography and geographical information system from Nanjing University, Nanjing, China, in 2009 and 2012, respectively.

He is the author of two articles. His research interests include land use and land cover change and remote sensing of snow.

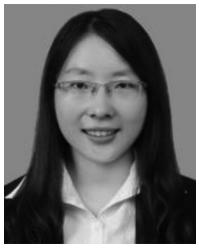

Xiaohui Wang was born in Hoshan, Anhui, China, in 1989. She received the B.E. degree in surveying and mapping engineering from the Anhui University of Architecture, Hefei, China, in 2010, and the M.S. degree in cartography and geographical information system from Nanjing University, Nanjing, China, in 2013.

She is the author of two articles. Her research interests include land use and land cover change.

Weiding Feng was born in Shanxi, China, in 1989. He received the B.S. degree in geographical information system from Shanxi University, Taiyuan, China, in 2011, and the M.S. degree in cartography and geographical information system from Nanjing University, Nanjing, China, in 2014.

He is the author of one article. His research interests include land use and land cover change.

Xiao Chang was born in Chuzhou, Anhui, China, in 1988. She received the B.S. degree in geographical information system from the Anhui Normal University, Wuhu, China, in 2011, and the M.S degree in cartography and geographical information system from Nanjing University, Nanjing, China, in 2014.

She is the author of one article. Her research interests include land use and land cover change.